AIAA AVIATION Forum
June 25-29, 2018, Atlanta, Georgia
2018 Atmospheric and Space Environments Conference

10.2514/6.2018-3654

An Experimental Study on the Durability of Icephobic Slippery Liquid-Infused Porous Surfaces (SLIPS) Pertinent to Aircraft Anti-/De-Icing

Liqun Ma[1], Zichen Zhang[2], Linyue Gao[3], Yang Liu[4] and Hui Hu[5](✉)
Department of Aerospace Engineering, Iowa State University, Ames, Iowa, 50011

Recently, bio-inspired surfaces have been found to be hydrophobic and/or icephobic, which has very low adhesion force for water and/or ice. When bio-inspired surfaces are applied for aircraft icing mitigation, they would suffer erosions due to high-speed impacting of the water droplets in the form of fog/mist. However, the knowledge of the coating durability regarding spray erosion is still quite limited. In the present study, an experimentally investigation was conducted to evaluate the durability of a PTFE membrane based slippery liquid infused porous surface (SLIPS) subject to water spray erosion, in comparison to that of a commonly used superhydrophobic surface (SHS) coating (i.e., a commercially-available Hydrobead® SHS coating). A wind driven spray generator was established with the spray erosion speed controllable from 45 m/s to 95 m/s. The anti-icing performance of the SHS and the SLIPS was validated in an icing research wind tunnel. Impact dynamics of individual water droplets at high Weber number about 3,000 and water spray erosion process of the SHS and the SLIPS were compared. The wettability-based coating lifetime was analyzed by measuring the dynamic contact angles on the SHS and the SLIPS under water spray erosions with different velocities. A cumulative-fatigue-damage theory was used to help predict the coating life time for in-flight aircraft icing mitigation. It turns out that the SLIPS could maintain its hydrophobicity better than the SHS under a moderate spray erosion speed. The mechanism of the spray erosion process for the SHS and the SLIPS was also examined in this study.

Nomenclature

CA	=	Contact angle, degree
D	=	Droplet diameter, m
D_{outlet}	=	Outlet diameter of the wind tunnel, m
LWC	=	Liquid water content, g/m^3
N	=	Count of droplet impingement
Q	=	Flow rate, m^3/s
U	=	Flow velocity, m/s
V	=	Droplet velocity, m/s
S	=	Spray impact area, m^2
T	=	Temperature, °C
Re	=	Reynolds number
We	=	Weber number
θ_c	=	Static CA, °
θ_a	=	Advancing CA, °
θ_r	=	Receding CA, °
θ_h	=	Hysteresis, °
ρ	=	Density of water, kg/m^3
σ	=	Surface tension, N/m
ν	=	Kinetic viscosity of air, m^2/s

[1] Graduate Student, Department of Aerospace Engineering.
[2] Graduate Student, Department of Aerospace Engineering.
[3] Graduate Student, Department of Aerospace Engineering.
[4] Post-Doctoral Research Associate, Department of Aerospace Engineering.
[5] Martin C. Jischke Professor, Department of Aerospace Engineering, AIAA Associate Fellow, Email: huhui@iastate.edu

I. Introduction

Ice accretion on inflight aircraft aerodynamic surfaces presents a severe and dangerous risk for aviation security. After the airplane takes off, especially in cold weather regions, it is the super-cooled droplets impingement onto the airfoil surface or engines that majorly lead to the severe icing problems. Icing on the airfoil or engine will do considerably harm to the aerodynamic performance of airplane and probably leads to aircraft accident [1, 2]. Nowadays, with the rapid development of the surface science and engineering, more and more bio-inspired hydrophobic/icephobic coatings have been designed[3] and many of them would have huge potentials to be applied in aircraft anti-icing scenarios.

Superhydrophobic surfaces owns contact angles above 150° and they are repellence to water. Wettability is one of the most fundamental properties of solid surface which is governed by the surface chemical composition and the microstructure morphology. The wing of butterfly Morpho aega[4], the feet of water starter[5] and the leaf[6] of lotus are typical natural superhydrophobic surfaces which give people inspirations to generate coatings with super-hydrophobicity. Superhydrophobic surface is an ideal passive anti-icing technique that its ice repellent performance has been proved is effective to mitigate ice accumulation. SHS have advantages such as low-cost ice-phobicity, easy to maintenance, light weight and environmental friendly. However, SHS will easily lose ice repellence ability after a short time use and is vulnerable to chemical corrosion, particle erosion and mechanical damages [7, 8, 9].

Slippery liquid-infused porous surfaces are well known for their pressure-stable omniphobicity[10], which means they are not only repellent to water (hydrophobic), but also repellent to ice (icephobic). The SLIPS are attracting great interest as a kind of anti-icing coating recently.[11–14] This kind of surfaces could reduce ice accumulation by allowing the condensed water droplets to slide off before they freeze. [10] The ice adhesion force on SLIPS is of 1-2 orders of magnitude lower compared to conventional materials [10,15,16], such that an easy removal of the ice formed on them can be achieved. The anti-icing performance is mainly achieved by using a slippery-oil layer in between the water and the solid substrate. Since it was found the anti-icing performance is almost independent of the underlying texture[10], the slippery lubricant plays an essential part in the anti-icing process. As a consequence, the lubricant depletion becomes a challenge for the longevity and durability for their implementation as icephobic surfaces. [14,3,17]

Traditional coating durability test mainly concerns the mechanical durability such as the adhesive durability, tangential abrasion durability, dynamic impact durability and liquid bath durability.[18] Most of them focus mainly on the damage of the solid surface morphology, which might impair the functioning mechanism such as loss of surface chemicals or hierarchical structures. However, when it comes to application of high-speed vehicle anti-icing, the SHS and the SLIPS might encounter severe water droplet erosions, which has not been fully investigated. Especially for SLIPS, the depletion of the slippery liquid seems to be the most significant form of surface degradation. The SLIPS might have considerable recovery ability from tape peeling or abrasion tests, but its ability to survive from liquid dynamic impact test is questionable.

Previous studies considering the water erosion durability always use relatively low impact velocities and large droplet sizes, and the speed of the spray impact is always not uniform. Liu *et al.* [16] conducted a rainfall test using a pressurized water spray for their lubricant-infused electrospray silicon rubber surface. The water droplets were 300 μm–3 mm in size, with the falling height ranging from 0.5 m to 2 m. It was indicated that with an increasing water flushing time, the contact angle hysteresis has increased and the freezing time on the test surfaces has decreased. Both the hydrophobicity and the icephobicity has been significantly degraded after ten hours' rainfall simulation. Other similar water spray durability tests were conducted by Davis *et al.* [19] (impact velocity 25 m/s), Xiong *et al.* [20] (impact velocity < 2 m/s) and Zhang *et al.* [21] (impact velocity 7.75 m/s). However, all the test condition mentioned above were simulating rainfall's influence on different surfaces. The droplet size was comparable to raindrops and the impact velocity was low. Water spray durability for SHS and SLIPS with finer droplet size and higher impact velocity are needed especially for scenarios when SHS or SLIPS were used as anti-icing surfaces for aircrafts or wind turbines, where the high-speed moving bodies might intercept with small droplets in clouds or atmospheric moisture.

In this study, we developed a new method to characterize the coating durability for the SHS and the SLIPS, which majorly focused on the coating erosion by water spray. We developed a high-speed spray system with controllable spray droplet speed to investigate the degrading process of the SHS and the SLIPS. Spray droplets with mean diameter around 8 μm can be accelerated up to 95 m/s during the spray erosion test. By applying water spray with different test durations, dynamic spray impact behaviors, impact velocities, surface properties such as the surface morphology and wettability were measured. It turns out that the SLIPS could maintain its hydrophobicity better than the SHS under a moderate spray erosion speed. The water repellent performance could be severely degraded when the microscopic structures were removed for the SHS and when the oil soaked into the porous layer was flushed away by the high-

speed spray droplets. Firstly, the anti-icing performance of the SHS and the SLIPS was validated in the ISU icing research wind tunnel. Secondly, impact dynamics of individual water droplet with Weber number around 3000 and water spray erosion behaviors on the SHS and the SLIPS were compared. Thirdly, the wettability-based coating lifetime was analyzed by measuring the dynamic contact angles on the SHS and the SLIPS with different erosion velocities. A cumulative-fatigue-damage theory was used to help predict the coating life time in in-flight aircraft anti-icing applications. Finally, the mechanism of the spray erosion for the SHS and the SLIPS was also generalized and compared. The mechanism of the spray erosion process for the SHS and the SLIPS was also compared in this study.

II. Experimental Methods

A. Wind tunnel for spray generation

In order to generate high-speed water spray for the durability test, a small wind tunnel was established. As shown in Figure 1, a metal ducted fan (JP 90mm 8s EDF) was used to control the wind speed. Using an electronic speed controller (ESC) (Platinum PRO V4) and an adjustable switching power supply (Volteq HY30100EX), the wind speed could be adjusted between 0 to 100 m/s. A spray system was established which includes a pneumatic spray nozzle (Ikeuchi BIMV11002), a pressurized water tank, pressure regulators, valves and tubes. The spray could be adjusted for its spray capacity by regulating the air pressure and the liquid pressure. A 3D printed nozzle holder could locate the nozzle downstream of the metal fan in the central axis of the tunnel, and the spray droplets can be fully mixed with the wind before flowing out of the outlet. The outlet had a diameter of 1 inch which was also 3D printed. The rest of the wind tunnel were made of standard PVC pipes and adapters. During the test, the test surface was mounted inside an acrylic target case, which could collect the water droplet after their collision with the test surface.

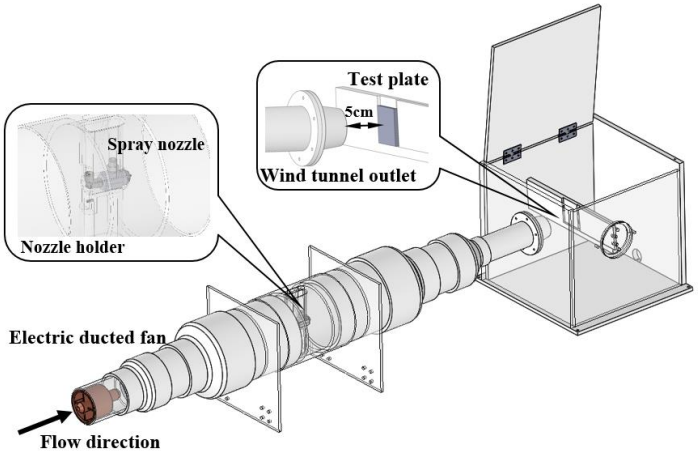

Figure 1. Schematic of the experimental setup for the spray generator.

B. Spray property measurement

We characterized the spray by controlling the air pressure and the water pressure for the nozzle. Fine fog-like spray was steadily generated. The droplet diameter distribution was measured with the Particle Master system (LaVision). By analyzing the shadow images of the droplets illuminated by a LED lamp (Veritas miniConstellation 120 28°), the droplet diameter was found to concentrated near 6 μm and the diameter range is about 4-30 μm.

A macro view of the spray property was achieved using Particle Image Velocimetry (PIV). The water droplets were used as the tracer particles directly. As shown in Figure 2, the flow of the spray had good symmetricity. The stagnation point inside the low speed region located in the center of the spray. The spray in the current test had a shape looks like circular cylinder after blown out from the wind tunnel's outlet, which is different from the shape as generated directly from the nozzle. It was indicated that by fixing the air and water pressure as the same, larger wind speed will lead to sparser impact droplets due to the fixed water flow rate Q. The LWC in this study would change with the wind speed U and their relation can be presented as:

$$LWC = c\frac{\rho Q}{U}, \tag{1}$$

where c is a constant related with the geometry of the wind tunnel.

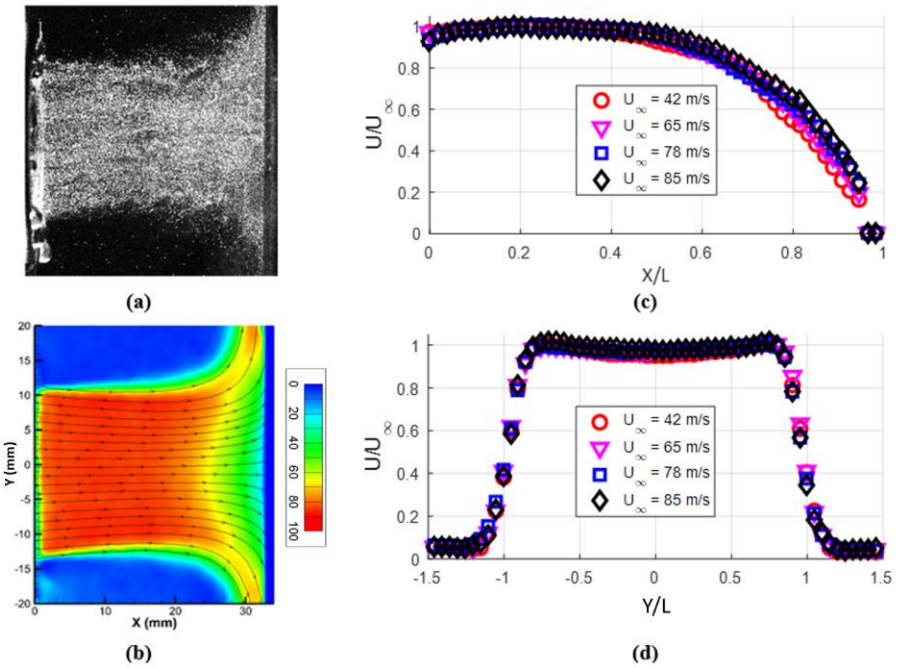

Figure 2. Spray property measured by PIV. (a) Image of the water spray illuminated by the laser sheet when U_∞ = 42 m/s. (b) Contour of the velocity magnitude field superposed with streamlines when U_∞ = 85 m/s. (c) Streamwise distribution of U/U_∞ at Y/L = 0. (d) Vertical distribution of U/U_∞ at X/L = 0.2.

C. Coating preparation

The SHS coating were made by spraying Hydrobead® on well-polished aluminum plates. Aluminum is polished with sandpaper grits ranging from 220 to 2000 and further with polishing compound to achieve mirror [22]. Both the Hydrobead® standard and the Hydrobead® enhancer were applied according to the instruction provided by the product. The distance from the spray gun to the target surface is a constant 9 inches to eliminate the difference of coating surface.

The porous layer of the SLIPS was made of a random network of Teflon nanofibrous membranes, which is commercially available from Sterlitech®. The hydrophobic membrane was laminated. Its functioning surface had an average pore size of ≥ 200nm and its polypropylene backer was sticked to an aluminum substrate. The lubricating fluids used for the experiments were DuPont Krytox 103, which is one kind of clear, colorless perfluorinated oil used by Wong *et al.*[10] and Liu *et al.*[16]. The slippery oil infused surfaces had a thickness of 60-80 μm.

Both SHS and the SLIPS were applied on 2" × 2" aluminum plates. It should be noted that the perfluorinated fluids selected for the SLIPS was Krytox® 103 since its low evaporation rate could eliminate the influence of oil depletion from evaporation. Wong et al [10] conducted a the evaporation measurement for the perfluorinated fluid by measuring the liquid mass loss with a high resolution balance (Mettler Toledo AT460 DeltaRange analytical balance with 0.1 mg sensitivity). They found that for the Krytox® 103, the evaporation rate is less than 0.05% per day and the changing of the surface wetting property is negligible within a 28-day period. With a similar test condition where the temperature is 20 °C and 50% relative humidity, we assume the durability change due to evaporation of the perfluorinated fluid is unimportant.

D. Contact angle measurement

High speed camera (PCO 1200hs camera) with a high 12x zoom lens system (LaVision) was used to record the static and dynamic CA. The commercial software of ImageJ was used to measure the CA information. Measurement of the static CA θ were performed by directly placing a 10 μL deionized water droplet over the test surfaces. The advancing CA $\theta_{adv.}$ and receding CA $\theta_{rec.}$ were measured by expanding and contracting a 50μL sessile droplet with a rate of 10 μL/s. The hysteresis is defined as the difference between $\theta_{adv.}$ and θ_{rec}. The water droplet was controlled by a Syringe pump (Genie Touch). The measurement was repeated at least three times for each experimental case to eliminate random error of the measurement.

III. Results and Discussions

A. Comparison of anti-icing performance of the SHS and the SLIPS

The anti-icing performance of three kinds of surfaces is compared in Figure 3 on the pressure side of the airfoil DU96-W-180. The test was completed inside an icing research wind tunnel at Iowa State University and detailed information could be referred to Liu *et al*[23]. Glaze ice was generated under *LWC* of 1.20 g/m^3 and temperature of -5 °C. The baseline case was applied with the coating of white enamel, which is hydrophilic. More ice was accumulated on the baseline case and there exist obvious iced rivulets, which are distributed from 0.25 to 0.5 of the chord length. In contrast, both SHS and SLIPS reduced water runback icing due to their super-hydrophobicity and hydrophobicity. In other words, water droplets are easier to roll away from the SHS and the SLIPS before freezing on the surface.

Even though the SHS and the SLIPS have better anti-icing performance than the baseline case, all the three surfaces have encountered ice accretion near the leading edge. After ice accretion on the leading edge, the impact ice will be formed on the ice surface, which means that a layer of ice would prevent the surface coating from damaged by the subsequent water spray or ice crystals. Note that the ice accretion on the leading edge was initialized almost at the same time within the first 30 seconds, while the water runback icing could be prevented for a much longer time on SHS and SLIPS.

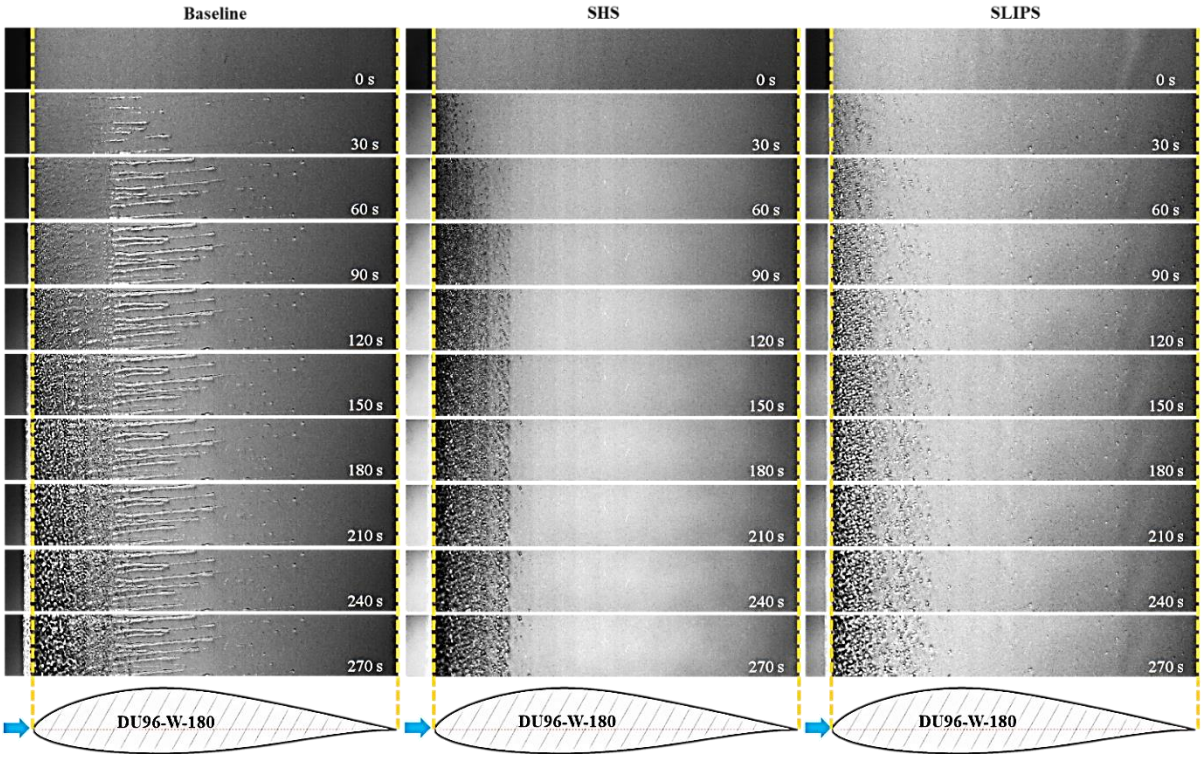

Figure 3. Comparison of dynamic ice accretion process over different surfaces on the DU96-W-180 airfoil under the glaze icing conditions. (Pressure side with U_∞ = 40m/s, T_∞ = -5 ºC, and *LWC* = 1.20 g/m^3).

B. Dynamic impinging process of water droplets at high Weber numbers

The impact dynamics of droplet with Weber number of 3000 are compared on the baseline surface, SHS and the SLIPS. This part of results were conducted in a wind tunnel which can accelerate the droplet, and the corresponding details could be found from the authors' other works[24,23]. The splashing phenomena was shared by the three surfaces in the very early stage at about 0.5 ms, while after which, the impact dynamics were very different on the three surfaces. On the hydrophilic baseline surface, water droplet would spread out as a water film with its maximum diameter remained on the surface. On the SHS, the droplet would sufficiently expand itself into a large water film, after which the water film broke up and rebound away from the superhydrophobic surface. On the SLIPS surface, the droplet will spread into a water film firstly, and then the water film receded back to the impact location. It should be noted that after the droplet impacting onto the SHS, a smaller droplet has penetrated the micron surface structures, and it finally remained in the center of the impact location. The receding process was accompanied by the breaking up process when multiple smaller droplets were generated. From the perspective of anti-icing, all the three surfaces had more or less water was remained at the impact location. This phenomenon is correlated with the results in Figure 3 when all the three cases had ice accreted on the leading edge. Since the SHS and SLIPS allows the water to easily roll away under the wind shear force before icing, the water runback icing can be prevented.

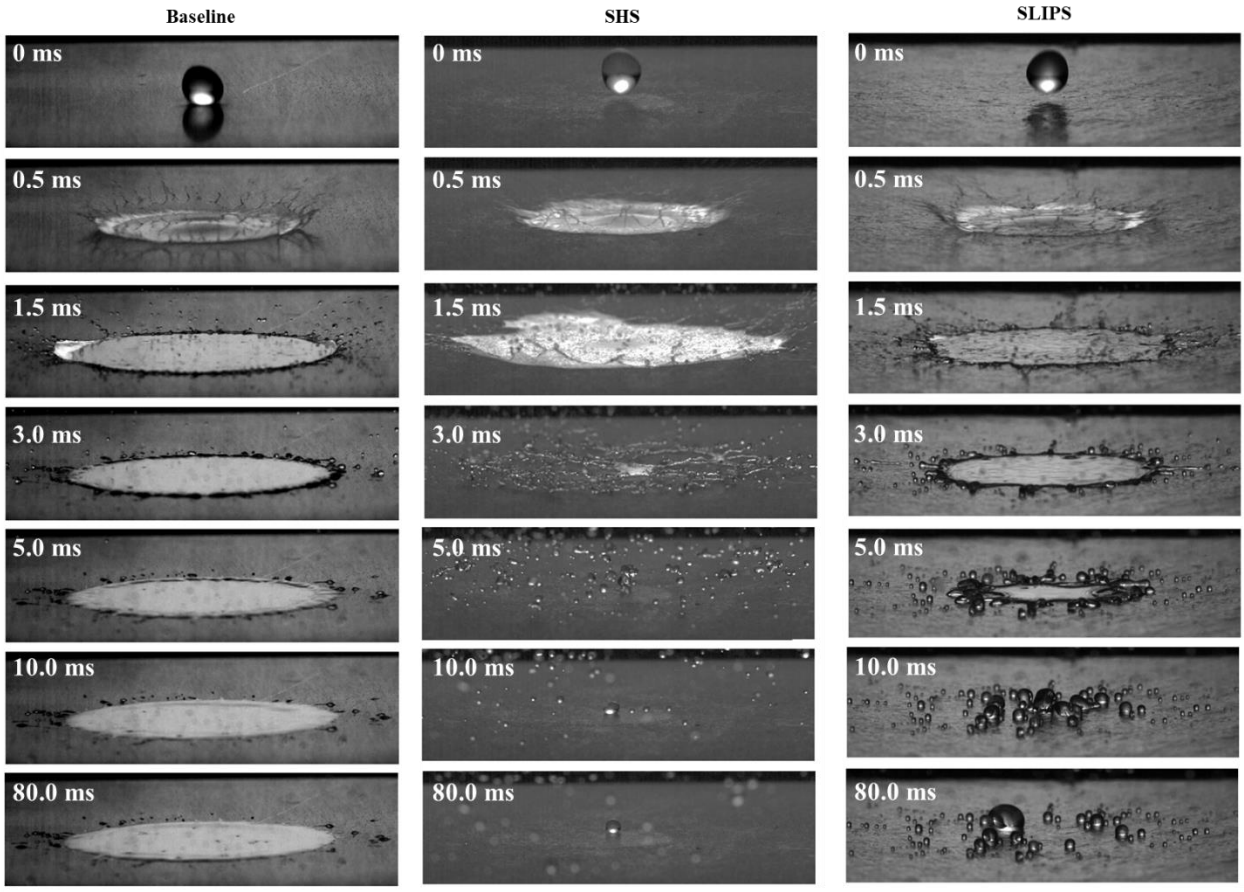

Figure 4. Comparison of water droplet impact dynamics onto (a) enamel coated surface, (b) SHS and (C) SLIPS. The droplet diameter is 3.1 mm and the impact velocity is 8.7 m/s (We = 3000), under room temperature.

C. Initial stage of the spray erosion

Figure 5 compares the initial stage of water spray erosion for the SHS and SLIPS. At a relatively low impact velocity and high *LWC* in this study, SHS and SLIPS behaves differently in the initial stage of the spray erosion. As shown in Figure 5(a), water spray generated a bright region in the center of the impact location. The reason is that before the impact of the spray, the hierarchical structure of the SHS would generate less light reflection. However, after the impingement of the spray, the hierarchical structures were saturated by the high-speed droplet and a water film is generated at the impact location. More light reflected from the aluminum substrate was allowed to go through the water film, and thus the bright spot was generated. It should be noted that the saturated water film would exist along with the water spray erosion regardless of the wind speed (from 45 m/s to 95 m/s). However, once the water spray was terminated, the water film will be rapidly evaporated by the upcoming wind and the local super-hydrophobicity could be regained.

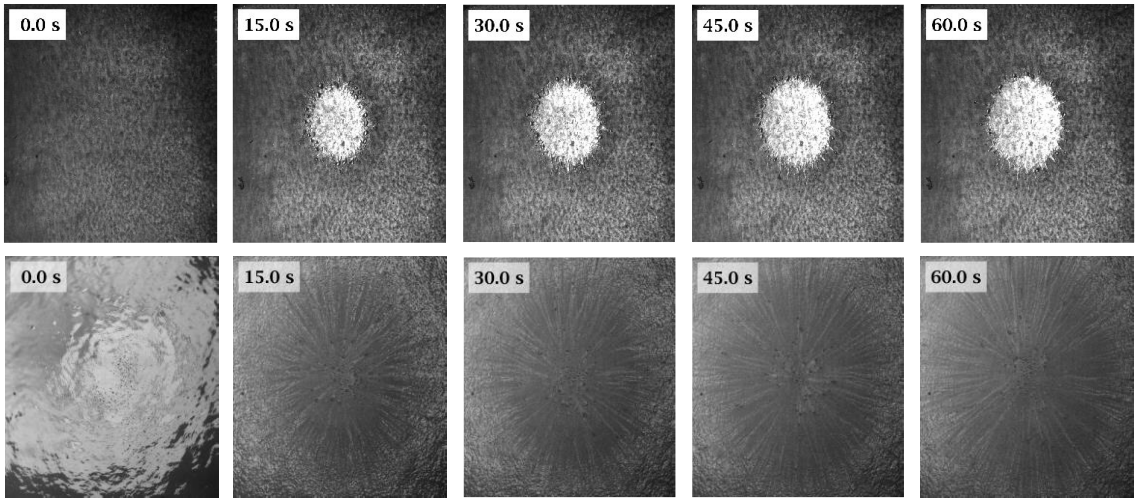

Figure 5. Initial stage of the water spray erosion on the SHS and the SLIPS when the U_∞ is 45 m/s, *LWC* is 22 g/m^3. (a) Spray erosion on the SHS, (b) Spray erosion on the SLIPS. Size of the FOV is about 1.5×1.5 inch

Figure 5(b) presents the original stage of water spray on the SLIPS. At the snapshot of 0 sec, a bright "mirror" reflection of the LED light was achieved from the smooth oil surface with a suitable optical setup. The SLIPS was originally designed to serve when excess oil was applied[10]. However, it is not necessarily to fill the SLIPS with excess oil since the oil film is vulnerable to dynamic pressures due to depletion. As shown in Figure 5(b), the excess oil could be easily flushed away by water spray erosion. It is the oil soaked into the porous structures that works for anti-icing applications. It is also visualized that the droplets will slide away from the stagnation point radially unless they were trapped inside the low speed region.

Results in Figure 5 and Figure 4 help to explain why icing on the leading edge coated with SHS and SLIPS was initialized almost at the same time with the hydrophilic surface. Even though the SHS and the SLIPS are water repellent, the SHS will have a saturated water film generated near the stagnation point, while the SLIPS has droplets trapped inside the low speed region near the stagnation point. After the ice layer was formed on the leading edge, the functionality of the SHS and the SLIPS will be blocked.

D. Surface topology of the SHS and the SLIPS

Figure 6 compares the microscopic surface topology for the SHS and the SLIPS, respectively. Different techniques were used since the oil infused SLIPS has a liquid infused surface, which is hard to be directly measured using Atomic Force Microscope (AFM). Figure 6 (a) and (b) shows the AFM scanned surface topology images of the SHS coating. Figure 6 (a) shows the non-damaged coating with the averaged-roughness, Ra, of 1219 nm. In Figure 6 (b), after 60 minutes impingement with a velocity of 65m/s, Ra dramatically decreases to 425 nm. The hierarchical structure has been damaged since the microscopic bulge structures no longer exist. The hydrophobicity performance is significantly

degraded since the hysteresis value has increased for more than 40°. It can be seen that after impingement, surface becomes flatter and coating material is removed gradually. Figure 6 (c) and (d) shows the Confocal Laser Scanning Microscopy (CLSM) scanned surface topology images for the SLIPS. The oiled region and the oil depleted regions were presented in the same field of view since. In Figure 6 (c) and (d), left-bottom of the field of view represents the refilled oil and right-top region shows the surface after spray erosion. The oil region might not provide valid thickness information due to the measurement principal related with light interferences. However, it turns out that the oiled region would have streaks distributed over the bright region from the raw optical image as shown in Figure 6 (d). Note the SLIPS is of one-order rougher than the SHS tested in this study. Excess oil will either totally cover the substrate membrane or remained inside the valleys of the microscopic structures. As limited by the measuring technique, the depletion process of the oil soaked into the nanoscopic porous structure was not measured in this study.

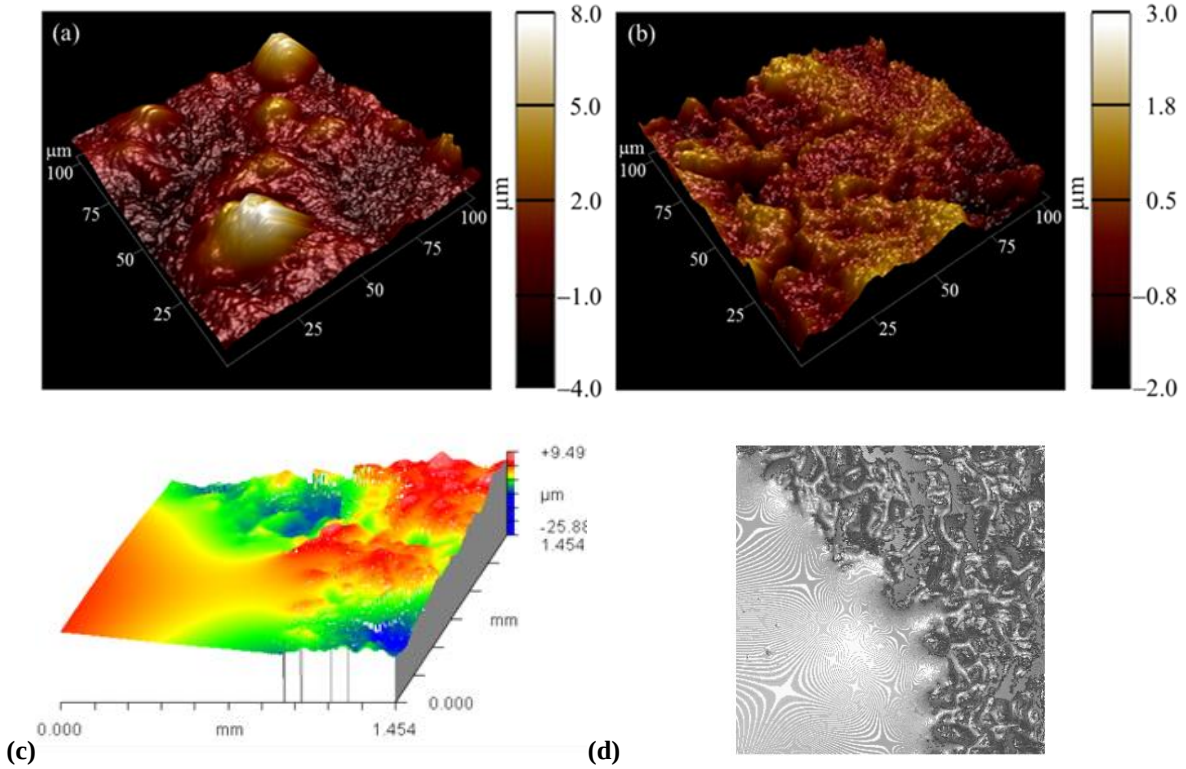

Figure 6. Comparison of surface topology of SHS and the SLIPS. AFM scanned surface topology images of SHS after droplets impingement with a velocity of 65m/s. (a) non-damaged, (b) after 60 min water spray erosion. CLSM scanned surface topology images for the SLIPS with the surface partially refilled with full oil. (c) 3D reconstructed surface profile (d) raw optical image correlated with (c).

E. Wettability based lifetime subject to spray impingement

After the initial stage of water spray erosion, no visible surface degradation could be detected until the macro structural defects are generated. In order to characterize the surface performance quantitatively, the surface wettability was measured at different spray erosion durations. We assume that only physical damages are caused to the surface and the damages is accumulated by repeated impingement of individual droplet of the same radius from the water spray. Since the *LWC* and the wind speed are correlated in this study, it is fairer to use the count of droplet impingement as the dimensionless time. Assume the droplet are perfectly sphere and they share the same radius *R*, the count of impingement is given by:

$$N = \frac{n\pi R^2}{S} \tag{2}$$

N could be understood as the number of duty cycles of the repeated damage of droplet impingement. The total number of droplets *n* can be calculated by using the ratio between the mass of the water released from the wind tunnel outlet and the mass of the individual droplet:

$$n = \frac{LWC \cdot t \cdot U \cdot S}{\frac{4}{3}\rho\pi R^3}. \tag{3}$$

Substituting *n* in Eq. 2, the count of droplet impingement can be expressed as:

$$N = \frac{3LWC \cdot t \cdot U}{4\rho R} \tag{4}$$

Given Eq. 1, *N* is linearly related with *t* for all the test case in this study since the flow rate of the spray system was maintained the same by fixing the nozzle's water pressure and air pressure as constants. To provide a reference point to calculate the *N*, we measured the *LWC* when the U_∞ is 65 m/s and the corresponding *LWC* is 15 g/m^3.

To achieve a parameter which could quantitatively represent the coating lifetime, both the static and the dynamic CA were measured. For the static CA, the SHS has a static CA decreasing with the spray erosion duration (from above 155° to below 135° when U_∞ is 95 m/s), while the SLIPS will retain its static CA as 112° ± 5° after a long duration of spray erosion. Static CA is thus not considered to serve as a general indicator of the coating lifetime in this study. For the dynamic CA, it was observed that both the SHS and the SLIPS would have their advancing CA kept steady. For all cases tested on SHS, the advancing CA is 165° ± 5°, and on the SLIPS the advancing CA is 115°±5°. As a result, the hysteresis variation is majorly determined by the receding CA according to its definition.

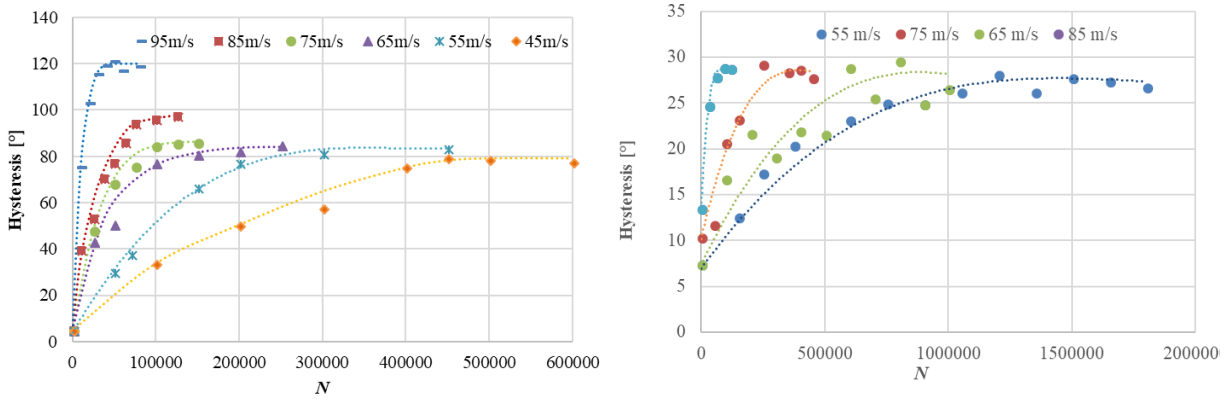

(a). SHS **(b).** SLIPS

Figure 7. Hysteresis variation as a function of count of droplet impingement on the SHS and SLIPS.

Figure 7 presents the hysteresis variation for the SHS and the SLIPS. Hysteresis will increase with the spray erosion time and finally reach a plateau, which means the water repellency of the SHS and the SLIPS would gradually degrade, and a steady state could be maintained after the degradation. Note that the SHS has its final hysteresis increased with the enlarging spray speed, while the SLIPS seems to have all the cases ended up with the same hysteresis. In addition, the change scale for the SHS (ranging from 75° to 115°) is much larger than that of the SLIPS (less than 25°). Under the same wind speed, the SLIPS appeared to be more durable than the SHS since more droplet impact duty cycles are needed for SLIPS to reach the steady hysteresis value.

We define N_0 as the wettability-based coating lifetime, and it is the count of droplet impingement *N* when the steady hysteresis is reached. Use the cumulative-fatigue-damage theory[25], we define a damage level *DL* to represent how close the current hysteresis state is to its final steady state.

$$DL = \frac{\theta_{h,current} - \theta_{h,initial}}{\theta_{h,final} - \theta_{h,initial}} \tag{5}$$

As shown in Eq. 5, the initial state has a *DL* = 0, which means no damage was generated to the surface wettability. While the final state has a *DL* = 1, which means the damage has been completed. Results in Figure 7 for both the SHS and the SLIPS could be nondimensionalized as a damage-cycle relationship as shown in Figure 8. By selecting suitable

N_0, all the hysteresis curves will collapse into one. Even though the uncertainty is rather large due to the large standard deviation value from the CA measurement, the trendlines fitted for all the cases either from the SHS or the SLIPS are very close to each other, which means the damage-cycle relationship is independent of the surface we applied. Current results shown no clue whether the damage-cycle relation is dependent on the spray impact velocity or not, since the deviations caused by the impact velocity could be a result from the measurement uncertainty or a bad selection of N_0.

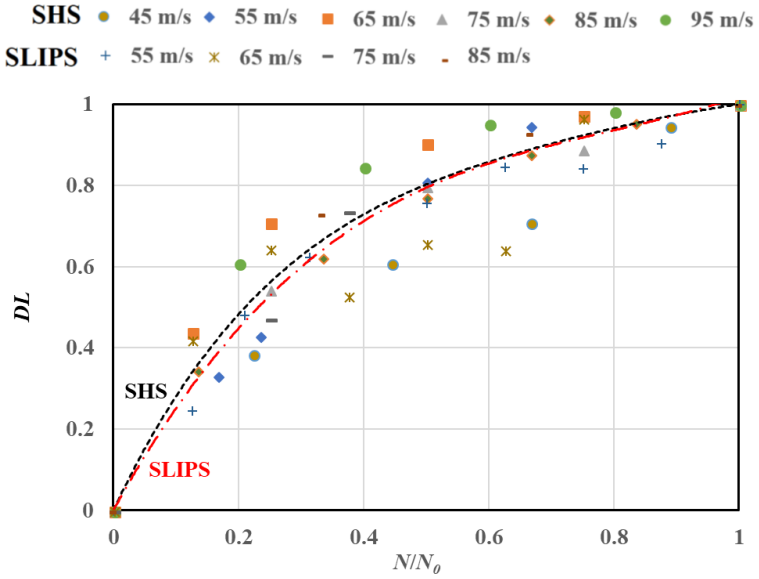

Figure 8. Damage-cycle relationship for the SHS and the SLIPS.

Figure 9 compares the wettability-based life time for the SHS and the SLIPS regarding the spray speed. The SLIPS is almost 3 times more durable than the SHS when the spray speed is less than 85 m/s according to the results from this study. Second order polynomials are used to fit the trendlines and there is no clue whether extrapolation of the relation works under spray speeds beyond the current experimental setup. However, this relation between N_0 and U_∞ can be helpful to the prediction of the coating lifetime for inflight-aircrafts using same coatings from this study. For example, given a specific wind speed U_∞, the corresponding wettability-related coating lifetime N_0 can be calculated. Plug back into N_0 and U_∞ Eq. 4, lifetime in t can be estimated given the LWC if the geometry of the droplets is similar.

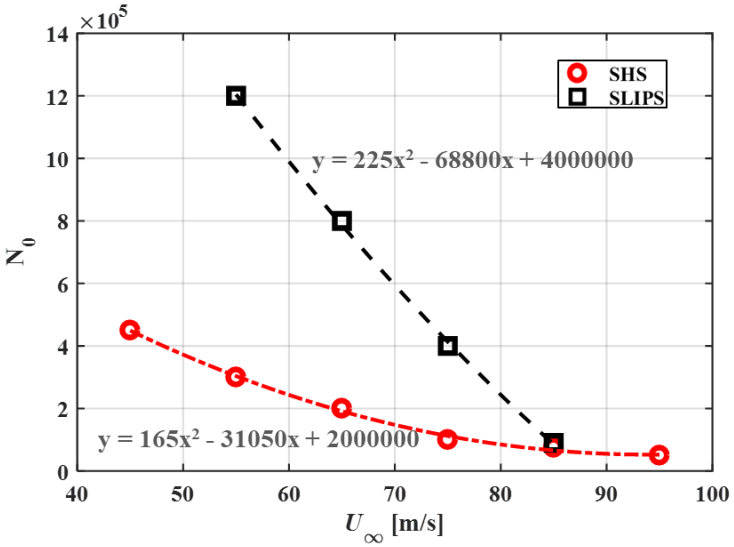

Figure 9. Comparison of wettability-based lifetime for the SHS and the SLIPS regarding spray speed.

F. Final surface damage styles

In this study, there is a visible structural damage to the SLIPS in the final stage of the water spray erosion. As shown in Figure 10, two sorts of surface damages styles are compared when the spray speed is 75 m/s. Images in the upper row and lower row present damage results for surfaces without and with slippery oil, respectively. Visible structural damage appears much earlier when no oil is applied, and the porous layer will be torn up by the water spray within 10 minutes. Three regions near the damage spot are selected to present the surface morphologies with a 40x magnification. Scopes A, B and C are corresponding to the regions of the undamaged surface, the edge and the center of the defect region. The original surface shown in Scope A has a relatively smooth texture, which represents the laminated PTFE membrane surface. As shown in Scope C, the porous layers have been smashed apart from the substrate layer, and the fragments of the porous layer after being blown to the edge of the defect spot are presented in Scope B. During the experiment, water could penetrate from the defect region and enter between the aluminum surface and the PTFE membrane.

Different from the results in the upper row, the PTFE membrane appears to be more durable after the slippery oil is applied. The oiled surface would be damaged after about 60 minutes of spray erosion. Moreover, the damage style is also different. As shown in Scope D, water has accumulated in between the porous layer and the substrate fabric. The evidence could be observed from the enlarged view of Scope E, where both air and water were trapped beneath the porous layer. Scope F presents the defect spot after 180 minutes' spray erosion. It is shown that with longer duration of spray erosion, more defect spots will appear. What's more, surface contaminations were observed as black dusts. These contamination dusts would accumulate on the SLIPS and the local wettability would be changed since theses dusts appeared to be hydrophilic.

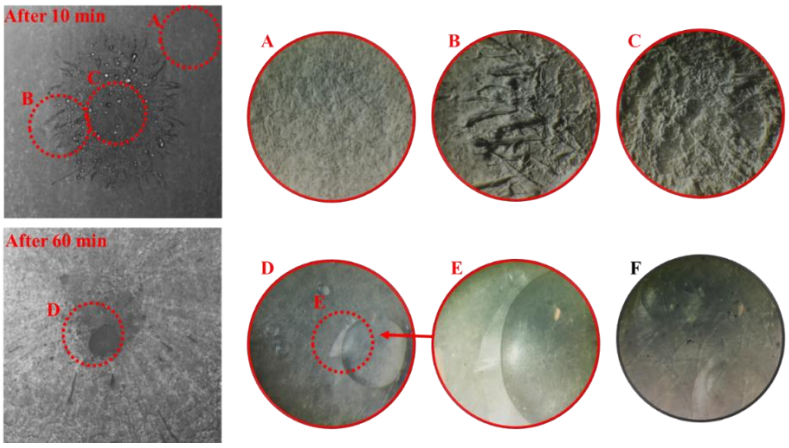

Figure 10. Typical surface damage styles for the SLIPS under water spray erosion (wind speed is 75 m/s)

G. Mechanism of the spray erosion for the SHS and the SLIPS

According to the previous discussion, the surface degradation mechanism of the spray erosion is generalized in Figure 11. For the Hydrobead® coated SHS, it is the micro- and nanoscopic architecture on the surface that can maintain the low hysteresis of the surface[26]. However, under water spray erosion, this hierarchical architecture is vulnerable to the repeated water droplets impingement. The damage of the microscopic mound-like structure of the SHS was visualized using AFM. Other indicators of the damage are represented by parameters of the surface wettability. An increased CA hysteresis was observed on the SHS and then the value of the hysteresis will reach a plateau, which was considered as a functional lifetime for the SHS. Longer time of water erosion would finally remove the coating from the substrate materials.

For the PTFE based SLIPS coating, the slippery oil plays an essential part to maintain its functionality. The extra oil applied to the PTFE laminates membrane could be rapidly removed either by the flow or the water spray. Thus, the water repellency is achieved by the nanoscopic porous structure with oil soaked inside. We assumed the oil depletion is the cause of the surface degradation according to the fact that the SLIPS could recover to its original state with oil refilled. In this study, even though the oil inside the porous layer is not effectively visualized, the degradation

of the SLIPS is measured according to the wettability information. Similar to the SHS surface, the SLIPS would also firstly have its CA hysteresis increases with the spray erosion time, and then reaches a plateau. When the SLIPS is left to the water erosion with a long time without refilling oil, the porous layer would either detach or be entirely removed from the substrate layer, and this kind of damage is unrecoverable.

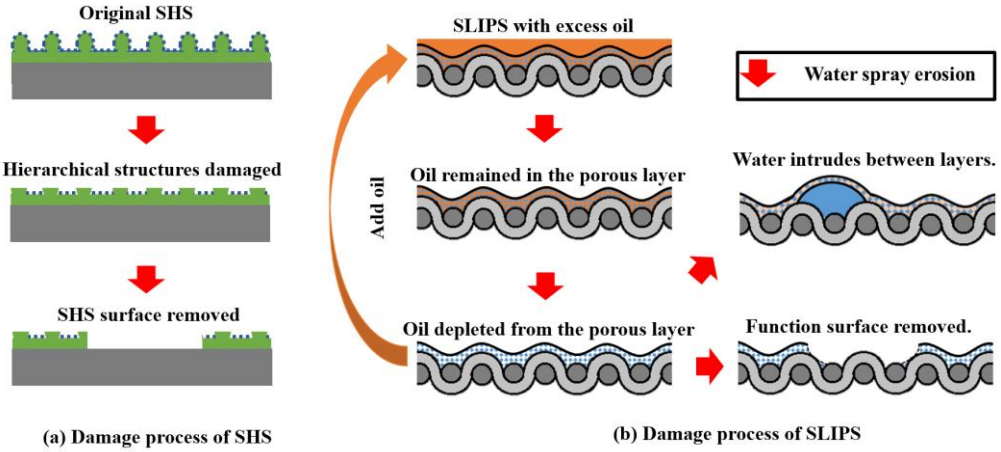

Figure 11. Mechanism of surface degradation by spray erosion for the SHS and the SLIPS.

IV. Conclusion

In summary, the durability of the Hydrobead® coated SHS and the PTFE-membrane-based SLIPS was tested and compared under water spray erosion. A small wind tunnel was established so that the spray speed could be controlled by a metal ducted fan. During the test, the droplet impact speed was varied from 45 to 95 m/s. The anti-icing performance of the SHS and the SLIPS was validated in comparison with the hydrophilic surface. The results indicate that the SHS and SLIPS coatings could effectively prevent the water runback icing under glaze ice condition. Droplet impact dynamics were also presented, which indicates that the low hysteresis of the SHS and SLIPS could allow more water to be blown away by the ambient wind after the impingement. By visualizing the early stage of water spray erosion on the SHS and the SLIPS, it was observed that both the SHS and the SLIPS are not repellent to spray impingement. It is because a saturated water film would be generated for the SHS and remained water droplet would be trapped in the low speed region near the stagnation point for the SLIPS. These findings could help to explain why the impact icing is inevitable, but the water runback icing could be effectively avoided.

Furthermore, the wettability-based coating lifetime is analyzed by measuring the dynamic contact angles on the SHS and the SLIPS under water spray erosions with different velocities. It was found that the advancing CA would remain almost the same during spray erosion. However, the hysteresis of the two kinds of coatings will gradually increase until a plateau was reached. According to this phenomenon, a dimensionless damage level was defined for the hysteresis based on the cumulative-fatigue-damage theory. By fitting the trendline for the relation between the wettability-based coating lifetime and the spray erosion velocity, helpful predictions for the coating lifetime applied for in-flight aircraft anti-icing was achieved. It turns out that the SLIPS could maintain its hydrophobicity better than the SHS under a moderate spray erosion speed. The mechanism of the spray erosion process for the SHS and the SLIPS was also compared in this study. Besides the traditional mechanical durability test, we suggest taking spray erosion test into consideration when the SHS and SLIP surfaces are applied into scenarios where high-speed water droplet erosion is present like application on vehicles, wind turbines and aircrafts.

Acknowledgments

The research work is partially supported by Iowa Space Grant Consortium (ISGC) Base Program for Aircraft Icing Studies, National Aeronautics and Space Administration (NASA) with the grant numbers of NNX16AN21A and NNX12C21A, and National Science Foundation (NSF) under award numbers of CBET1064196 and CBET1435590. The authors gratefully acknowledge the help and discussions from Dr. Ren, Dr. Bastawros and Mr. Dawood during the surface topology measurement.

References

[1] Liu, Y., Li, L., and Hu, H., "An Experimental Study on the Transient Heat Transfer and Dynamic Ice Accretion Process over a Rotating UAS Propeller," *9th AIAA Atmospheric and Space Environments Conference*, 2017.

[2] Liu, Y., Li, L., Ning, Z., Tian, W., and Hu, H., "Experimental Investigation on the Dynamic Icing Process over a Rotating Propeller Model," *AIAA Journal of Power and Propulsion*, 2018, pp. 1–15.

[3] Lv, J., Song, Y., Jiang, L., and Wang, J., "Bio-Inspired Strategies for Anti-Icing," *ACS Nano*, vol. 8, Apr. 2014, pp. 3152–3169.

[4] Feng, B. L., Li, S. H., Li, Y. S., Li, H. J., Zhang, L. J., Zhai, J., Song, Y. L., Liu, B. Q., Jiang, L., Feng, L., Li, S. H., Li, Y. S., Li, H. J., Zhang, L. J., Zhai, J., Song, Y. L., Liu, B. Q., Jiang, L., and Zhu, D. B., "Super-hydrophobic surfaces: From natural to artificial," *Advanced Materials*, vol. 14, 2002, pp. 1857–1860.

[5] Hu, D. L., Chan, B., and Bush, J. W. M., "The hydrodynamics of water strider locomotion," *Nature*, vol. 424, 2003, pp. 663–666.

[6] Zhang, J., Wu, L., Li, B., Li, L., Seeger, S., and Wang, A., "Evaporation-Induced Transition from Nepenthes Pitcher-Inspired Slippery Surfaces to Lotus Leaf-Inspired Superoleophobic Surfaces," *Langmuir*, vol. 30, Dec. 2014, pp. 14292–14299.

[7] Slot, H. M., Gelinck, E. R. M., Rentrop, C., and Van der Heide, E., "Leading edge erosion of coated wind turbine blades: Review of coating life models," *Renewable Energy*, vol. 80, 2015, pp. 837–848.

[8] Ishizaki, T., Masuda, Y., and Sakamoto, M., "Corrosion resistance and durability of superhydrophobic surface formed on magnesium alloy coated with nanostructured cerium oxide film and fluoroalkylsilane molecules in corrosive NaCl aqueous solution," *Langmuir*, vol. 27, 2011, pp. 4780–4788.

[9] Xiu, Y., Liu, Y., Hess, D. W., and Wong, C. P., "Mechanically robust superhydrophobicity on hierarchically structured Si surfaces," *Nanotechnology*, vol. 21, 2010.

[10] Wong, T.-S., Kang, S. H., Tang, S. K. Y., Smythe, E. J., Hatton, B. D., Grinthal, A., and Aizenberg, J., "Bioinspired self-repairing slippery surfaces with pressure-stable omniphobicity.," *Nature*, vol. 477, 2011, pp. 443–7.

[11] Stamatopoulos, C., Hemrle, J., Wang, D., and Poulikakos, D., "Exceptional Anti-Icing Performance of Self-Impregnating Slippery Surfaces," *ACS Applied Materials & Interfaces*, vol. 9, Mar. 2017, pp. 10233–10242.

[12] Chen, J., Dou, R., Cui, D., Zhang, Q., Zhang, Y., Xu, F., Zhou, X., Wang, J., Song, Y., and Jiang, L., "Robust Prototypical Anti-icing Coatings with a Self-lubricating Liquid Water Layer between Ice and Substrate," *ACS Applied Materials & Interfaces*, vol. 5, May 2013, pp. 4026–4030.

[13] Rykaczewski, K., Anand, S., Subramanyam, S. B., and Varanasi, K. K., "Mechanism of Frost Formation on Lubricant-Impregnated Surfaces," *Langmuir*, vol. 29, Apr. 2013, pp. 5230–5238.

[14] Kreder, M. J., Alvarenga, J., Kim, P., and Aizenberg, J., "Design of anti-icing surfaces: smooth, textured or slippery?," *Nature Reviews Materials*, vol. 1, Jan. 2016, p. 15003.

[15] Vogel, N., Belisle, R. A., Hatton, B., Wong, T.-S., and Aizenberg, J., "Transparency and damage tolerance of patternable omniphobic lubricated surfaces based on inverse colloidal monolayers," *Nature Communications*, vol. 4, Jul. 2013, p. 2176.

[16] Liu, Q., Yang, Y., Huang, M., Zhou, Y., Liu, Y., and Liang, X., "Durability of a lubricant-infused Electrospray Silicon Rubber surface as an anti-icing coating," *Applied Surface Science*, vol. 346, 2015, pp. 68–76.

[17] Sojoudi, H., Wang, M., Boscher, N. D., McKinley, G. H., and Gleason, K. K., "Durable and scalable icephobic surfaces: similarities and distinctions from superhydrophobic surfaces," *Soft Matter*, vol. 12, 2016, pp. 1938–1963.

[18] Milionis, A., Loth, E., and Bayer, I. S., "Recent advances in the mechanical durability of superhydrophobic materials," *Advances in Colloid and Interface Science*, vol. 229, Mar. 2016, pp. 57–79.

[19] Davis, A., Yeong, Y. H., Steele, A., Loth, E., and Bayer, I. S., "Nanocomposite coating superhydrophobicity recovery after prolonged high-impact simulated rain," *RSC Advances*, vol. 4, 2014, pp. 47222–47226.

[20] Xiong, L., Kendrick, L. L., Heusser, H., Webb, J. C., Sparks, B. J., Goetz, J. T., Guo, W., Stafford, C. M., Blanton, M. D., Nazarenko, S., and Patton, D. L., "Spray-Deposition and Photopolymerization of Organic–Inorganic Thiol–ene Resins for Fabrication of Superamphiphobic Surfaces," *ACS Applied Materials & Interfaces*, vol. 6, Jul. 2014, pp. 10763–10774.

[21] Zhang, Y., Ge, D., and Yang, S., "Spray-coating of superhydrophobic aluminum alloys with enhanced mechanical robustness," *Journal of Colloid and Interface Science*, vol. 423, 2014, pp. 101–107.

[22] Beeram, P. S. R., "Characterization of ice adhesion strength over different surfaces pertinent to aircraft anti-/de-icing," *Graduate Theses and Dissertations*, Jan. 2017.

[23] Liu, Y., Ma, L., Wang, W., Kota, A. K., and Hu, H., "An experimental study on soft PDMS materials for aircraft icing mitigation," *Applied Surface Science*, vol. 447, Jul. 2018, pp. 599–609.

[24] Ma, L., Li, H., and Hu, H., "An Experimental Study on the Dynamics of Water Droplet Impingement onto Bio-inspired Surfaces with Different Wettabilities," *55th AIAA Aerospace Sciences Meeting*, Grapevine, Texas: 2017, p. AIAA 2017-0442.

[25] Kaechele, L., "Review and Analysis of Cumulative-Fatigue-Damage Theories," 1963.

[26] Cheng, Y. T., Rodak, D. E., Wong, C. A., and Hayden, C. A., "Effects of micro- and nano-structures on the self-cleaning behaviour of lotus leaves," *Nanotechnology*, vol. 17, Mar. 2006, pp. 1359–1362.